Titania Nanoparticles Prepared with Pulsed Laser Ablation of Rutile Single Crystals in Water

Akira Iwabuchi,[†] Cheow-keong Choo,[‡] and Katsumi Tanaka*[,‡]

Graduate School of Electronic Engineering and Department of Human Communication, The University of Electro-Communications, 1-5-1 Chofu Tokyo 182-8585, Japan

Received: February 22, 2004; In Final Form: May 10, 2004

The pulsed laser ablation (PLA) experiments of rutile single crystal surfaces were carried out in water solution to prepare nanosized titania particles. The solvated PLA species were transparent as produced and changed to a lighter blue solution with some precursors for filamentous species (in several days), then finally changed to white enlarged filamentous species (in 2−4 weeks). The solvated PLA species were measured as uniform nanoparticles with a size below 10 nm by TEM measurements and showed the absorption−photon energy relation for the direct transition with a band gap of 5.3−5.5 eV. The band-gap values were elucidated with quantum confinement size effects. It was assumed that the primary solvated species should have a size of about 1 nm and they were agglomerated to be the secondary species. The Mie scattering is responsible for the "blue" color, which proves that the size enlargement process exists on the PLA species in water. The filamentous species are composed of mainly the anatase form, which was analyzed with Raman spectroscopy. The XPS results indicate that the Ti species are tetravalent and bonded to oxygen atoms with O 1s binding energy at around 530 eV as TiO_2. They were found to be composed to about 1 μm diameter with gathering nanosized particles on SEM pictures. The thin films composed of the PLA filamentous species showed no band gap increase. The process for PLA of rutile in water was studied with different temperatures (T in K) to elucidate the effect of viscosity (η). The yield of PLA species in water decreases nearly linearly with the ratio of T/η representing the diffusion coefficient of the solvated species. The result implies that the PLA species are confined in a media not diffused into water solution.

Introduction

Titania has gained much interest as an advantageous semiconductor material not only for solar energy usage[1] but also for environmental sanitation.[2−4] Organic/inorganic hybrid solar cells have been considered favorable in place of inorganic cells since the discovery of dye-sensitized nanocrystalline TiO_2 photovoltaic cells with an overall energy conversion efficiency of about 7−10%.[5−8] The principles of heterogeneous titania photocatalysis have been reviewed[9] and photocatalytic activities on various materials can be compared by a mathematical description.[10] Practical photocatalytic systems in water environments are reviewed[11] and recently the titania/water system has been applied to reductive dechlorination of organic compounds under irradiation.[12] The band-gap energy of n-TiO_2 was lowered by doping transition metals,[13] nitrogen atoms,[14] and sulfur atoms[15] and the optical absorption edges were shifted to visible regions. Although photodegradation of organic compounds was successful at a wavelength λ <500 nm, direct water splitting was unsuccessful under irradiation. Efficient photochemical water splitting just recently succeeded on a flame pyrolysis chemically modified n-type TiO_2, whose band-gap energy was minimized to 2.32 eV to absorb visible light.[16] Furthermore, titania has been reported to be a suitable catalyst support, especially as the only support for heterogeneous molybdenum olefin metathesis catalysts with no hydrogen scrambling on which the reaction mechanism could be studied,[17−20] as well as suitable for the CO_2 dissociation on Pt to occur as a result of carbonate species being held on the titania support.[21]

Nanophase TiO_2 has been studied for the applications to nonlinear optical devices,[22] information storage,[23] and frequency doubling.[24] The anatase film showed the (101) plane as the most exposed face in nanocrystals.[22] However, the (110) face has been shown to be the exposed plane in the case of rutile. Then, the (110) plane yields a defect stoichiometry leading to Ti^{3+} site, which is photochemically active.[25] Titania synthesis has been summarized as (i) Ti-alkoxide precursors in aqueous[26,27] and organic media,[28] or in acid solution,[29] (ii) $TiCl_4$ hydrolysis at low temperature,[17,30,31] and (iii) a non-hydrolytic combination of Ti-alkoxide and $TiCl_4$.[32] Basically similar TiO_2 preparation methods have been applied to the nanoparticles, whereas nanofibers of anatase with controllable diameters and porous structure are prepared with electrospinning.[33] In addition, nanocrystalline spongelike porous TiO_2 foam can be synthesized by the reaction of hydrogen peroxide inside TiO_2/hexadecylamine slurry dispersion[34] and crystalline titania nanorings are prepared by using macroporous polymers as a template.[35]

Pulsed laser ablation (PLA) or pulsed laser deposition (PLD) as the applied method for preparing thin films has been widely applied not only to inorganic metal oxides but also to organic polymers.[36−40] One of the advantages in PLA or PLD methods is that stoichiometric thin films can be supplied with the same composition as the target materials. However, the synthesis of the multicomponent complex metal oxide films with use of targets composed of more than two single metal oxides is also

* Address correspondence to this author. Phone: 0424-43-5147. Fax: 0424-43-5566. E-mail: tanaka@hc.uec.ac.jp.
[†] Graduate School of Electronic Engineering.
[‡] Department of Human Communication.

10.1021/jp049200d CCC: $27.50
Published on Web 06/19/2004

possible as a new concept of the PLD method.[41−46] Non-stoichiometric PLD films can be prepared on which new functions will be expected. The photochemical NOx decomposition rate was increased on titania films with plasma treatment, which suggests that oxygen vacancies play an important role in the decomposition.[47] In fact, the plasma-treated PLD films showed higher dye decomposition rates.[48] Rutile and anatase films can be selectively prepared by reactive sputtering and well-characterized optically as well as electrically.[49] The electrical studies on the prepared metastable anatase films show high donor concentrations and indicate a larger effective Bohr radius of donor electrons, which suggests a smaller electron effective mass supported by the high mobility. Nanoparticles of the anatase phase can also be fabricated with oxygen-supplied PLD methods.[50] The PLDs of rutile TiO_2 yield rutile/anatase mixture nanocrystallines with a diameter below 30 nm,[51] TiOx nanoparticles such as Ti_3O_5 prepared by size selection, using differences in their electrical mobility[52] and brookite-rich thin films.[53] In addition, Pt/TiO_2 nanocomposite thin films prepared with PLD methods show unique optical properties: a photoluminescence emission at 650−870 nm,[54] photoelectrochemical response to visible light,[55] and most significantly an optical band-gap less than that of pure TiO_2.[56,57] The Pt/TiO_2 films can also be prepared with the PLD by using 2-beams.[58]

So far not only semiconductor nanocrystals[59−64] but also metal nanoparticles[65,66] have been studied because of their characteristic properties depending on the size. Metal nanoparticles have been prepared with PLA in water solution and their sizes are controlled by adsorption of ions or surfactants.[67−69] The PLA in the gas phase will involve the initial fragmentation of the bulk materials and the successive reconstruction of fragmented species during the flight path or on the substrate. The kinetic energies of flying species in the gas phase will be extremely high so that they collide with high-pressure gas-phase molecules and nanocrystalline species can be prepared as a result of relaxation. The PLA in solution will be quite different and it will be interesting to understand the following questions: (1) how the initial fragmented species react with solution molecules to become relaxed, (2) how the reaction media in the liquid phase plays a role on the nature and the size of species, (3) how the reconstruction of fragmented species occurs, and (4) how the reconstructed species are terminated. If the charged species are formed in water, the surface will control the stability of solvated species which should be responsible for the propagation step to yield clusters. The structure of nanospecies whether rutile or anatase is also significant to study. In the present paper, the first trial of TiO_2 nanoparticles preparaed with PLA of rutile single crystals in water is reported. The PLA species are studied with UV−vis spectroscopy, transmission electron microscopy (TEM), Raman spectroscopy, secondary electron microscopy (SEM), and X-ray photoelectron spectroscopy.

Experimental Section

A commercially available rutile TiO_2 single-crystal rod was sliced to a disk of about 8-mm diameter with a thickness of about 2−3 mm. The disk surface was mechanically polished and further cleaned ultrasonically with distilled water, isopropyl alcohol, and acetone, repeatedly. No special oriented surface was used. The pulsed laser ablation (PLA) of the sliced rutile pellet was carried out in distilled water. The fourth harmonics (266 nm, 10 Hz) of a Nd:YAG pulsed laser (Continuum, Surelite-10) were reflected with the mirror and vertically supplied to the pellet. The laser light was focused with a quartz lens with a focal length of 150 mm. The energy density, so-called fluence, was estimated from the supplied laser energy and the spot size. The laser energy was measured with a laser power meter (OPHIR, model AN/2). The laser light was focused to a burn paper at the same conditions as for PLA experiments and the spot size was detected with an optical microscope. Typically the laser energy (20 mJ) and the spot size(2×10^{-4} cm^{-2}) correspond to a laser fluence of 100 Jcm^{-2}.

The absorption spectra were recorded with a UV−vis spectrophotometer (JASCO U-best-30) with quartz cells. The particle size of the PLA species with an absorption peak at around 200 nm was measured with transmission electron microscopy (TEM: Hitachi JEM-4000 Ex-II). Surface morphologies of the ablated rutile surface and the filamentous PLA species were studied with a secondary electron microscope (SEM) by an electron probe micro analysis, EPMA (JEOL JCXA-733) and FE-SEM (JEOL JSM-6340F), respectively. For SEM pictures the sample surfaces were coated with evaporated carbon. The crystal structure of the filamentous PLA species was studied with Raman spectroscopy (JOBIN YVON U-1000) at 514.5 nm with use of an Ar ion laser of 200 mW and a beam diameter of 100 μm. The effect of focused laser power on the crystallization was negligible since the amorphous titania film showed no change in the same Raman conditions. Core level photoelectron spectra were recorded with X-ray photoelectron spectroscopy (XPS; VG-ESCA Lab 5), in which Al Kα radiation (1486.6 eV) at 50 W anode power and a pass energy at 50 eV were employed. The charge-up of binding energy (BE) values was referenced to the C 1s peak at 285.6 eV as an internal standard. Then, BE values of Ti $2p_{3/2}$ and O 1s on a commercially available rutile (010) surface were 458.9 and 530.0 eV, respectively. These values are quite reasonable and almost the same values as reported.[21] The "scattering" of the blue PLA solution was studied as follows. If the scattering occurs in the PLA solution, the light intensity of the applied wavelength should be enhanced. This was the case in our experiments. The PLA solution in the qualtz cell was placed in UV−vis spectroscopy and the whole system was put in a light-screened black box. The 150-W Hg−Xe lamp irradiated the blue solution. The scattered light was so weak that it was integrated for 30 min with a multichannel photodetector (Hamamatsu photonics PMA-11.C7473−36) placed 90° off the Hg−Xe lamp. The intensities of the solution in PLA experiments were increased by scattering at the wavelengths of the Hg−Xe line spectra and were referenced to those of distilled water as their ratios. The intensity increases from scattering at the wavelengths of Hg−Xe line spectra are represented as their ratios. The scattering can typically be evaluated at some wavelengths at which the Hg line spectra are observed.

Results and Discussion

For simplification, the PLA species formed in the pulsed laser ablation of the rutile single crystal surface in water solution are summarized as follows. The solvated PLA species are transparent as produced (denoted as species A), change to blue with some precursors for filamentous species (species B), then finally change to white enlarged filamentous species (species C). As mentioned later species A are analyzed as homogeneously dispersed species sized uniformly below 10 nm with TEM pictures and the enlarged species are analyzed with XRD and XPS as titania species. Therefore in this article, the PLA species formed in water, blue solvated species with some precursor for filamentous species, and the enlarged filamentous species are all assumed to be titania species. Scattering experiments also

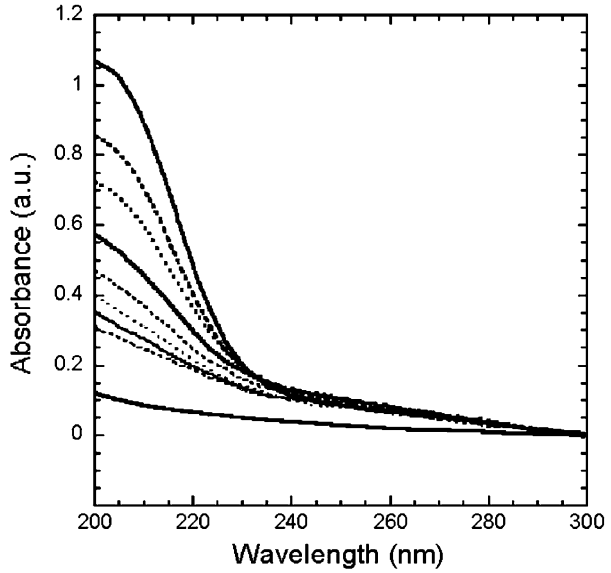

Figure 1. The UV−vis absorption spectra of the solution during the PLA of rutile in water. The spectrum lines represent measurements from 30 min (second bottom) to 4 h (top) at 30-min intervals. The bottom represents the blank water UV−vis spectrum (at time zero). The solid and dotted lines are used just for viewing. The PLA experiment was carried out in 10 mL of water at 298 K with laser fluence at 40 J cm^{-2} of 10 Hz.

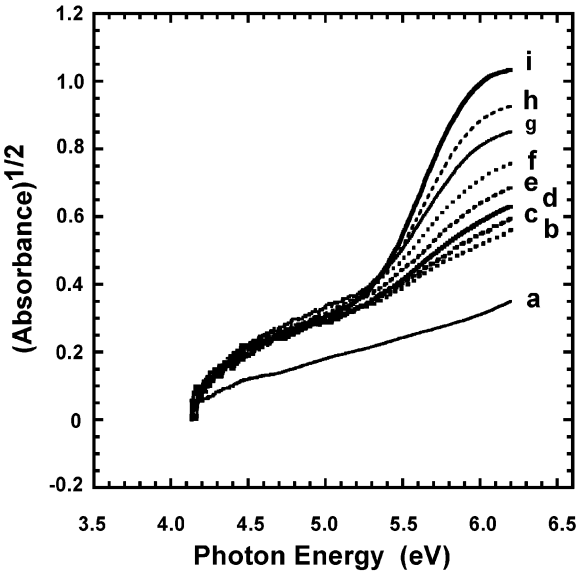

Figure 2. The square roots of absorbance in Figure 1 are plotted as a function of photon energy for the indirect transitions. The absorption spectra were measured from 30 min (b) to 4 h (i) at 30-min intervals. Spectrum a represents absorption of water at time zero.

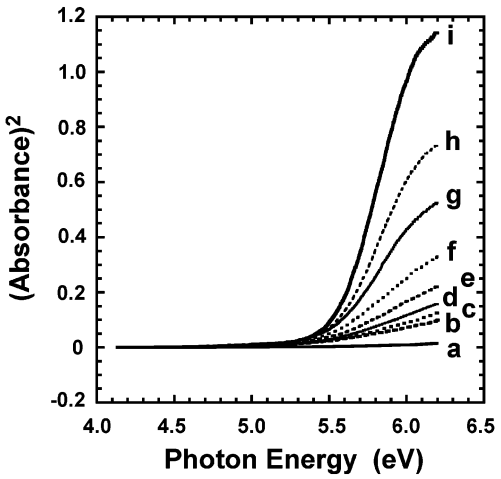

Figure 3. The square values of absorbance in Figure 1 are plotted as a function of photon energy for the direct transitions. The absorption spectra were measured from 30 min (b) to 4 h (i) at 30-min intervals. Spectrum a represents absorption of water at time zero.

suggest that the solvated species are nanometer sized and SEM pictures directly detect nanosized titania species as secondary particles.

When the PLA of the rutile single crystal surface is carried out in water, the solution is transparent but absorbance below 230 nm gradually increases with PLA time as shown in Figure 1. The absorbance between 230 and 300 nm seems saturated at 30 min. Here 10 mL of water was used and the laser fluence was about 40 J/cm^2. To evaluate the species formed in Figure 1, the absorption values are plotted as a function of photon energy. For the indirect transitions between indirect valleys (eq 1) and for allowed direct transitions (eq 2) of materials with band gap E_g, the absorbance values α are proportional to the square root and the square of photon energy, respectively.[70]

$$\alpha(h\nu) = C(h\nu - E_g)^2 \quad (1)$$

$$\alpha(h\nu) = D(h\nu - E_g)^{1/2} \quad (2)$$

As shown in Figure 2, the square root of the absorbance for the species between 230 and 300 nm (5.4−4.2 eV) can be extrapolated to about 3.2 eV as a function of photon energy. The result implies that the species could be rutile (E_g = 3.2 eV) particles directly ablated on the target. However, it was difficult to estimate E_g values for the PLA solvated species observed below 240 nm in Figure 1 because straight lines could not be obtained for these species in $h\nu-\alpha^{1/2}$ relations in Figure 2. It can be imagined that absorption edges are below 240 nm in Figure 1. This means that E_g reaches above 5 eV. If such species are solvated ions or clusters, the absorption should obey direct transitions because of a small difference of wave vector **k**. The plots of $h\nu-\alpha^2$ relations in Figure 3 clearly imply that the PLA solvated species A show direct absorption transitions. The E_g values can be obtained as 5.3−5.5 eV by extrapolating the α^2 values to zero. This fact implies that the same solvated species A are formed homogeneously with the PLA of rutile targets in water. The amount of the species can be estimated by the absorption value at 200 nm. The yield of the PLA in water is studied as a function of the PLA time in Figure 4. The absorbance at 200 nm was obtained by subtracting the absorbance of reference water from UV spectra after the PLA. This increases nonlinearly with the PLA time and the value extrapolated to zero is about 0.30. The nonlinearity implies that the species A formed in the PLA of rutile in water becomes easier to desorb as the PLA time increases. It will be associated with the fact that the rutile target surface seems to be ablated initially of the PLA experiments. The value extrapolated to time zero is directly related to the species B detected around 230−300 nm, which saturates at the early stage of the PLA.

Figure 5 shows the SEM picture of the rutile TiO_2 single-crystal target after 4 h of the PLA experiment in Figure 1. The ablated hole with diameter about 30 μm is seen on the single-crystal surface. The depth is very shallow because the submonolayer is removed at 1 pulse in most PLA or PLD thin film preparation processes.[46] It is significant to note that the periphery of the hole is piled up with small grains of diameter below 10 μm. The precursor species formed in the rutile PLA will remain on the surface and change to the deposited grains. If they are

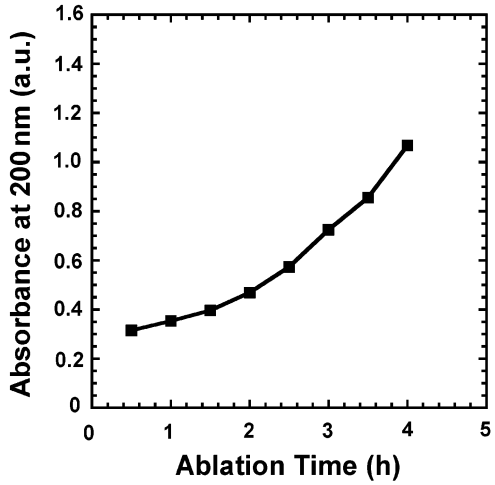

Figure 4. The values of absorbance at 200 nm as a function of PLA time. The results of Figure 1 are plotted.

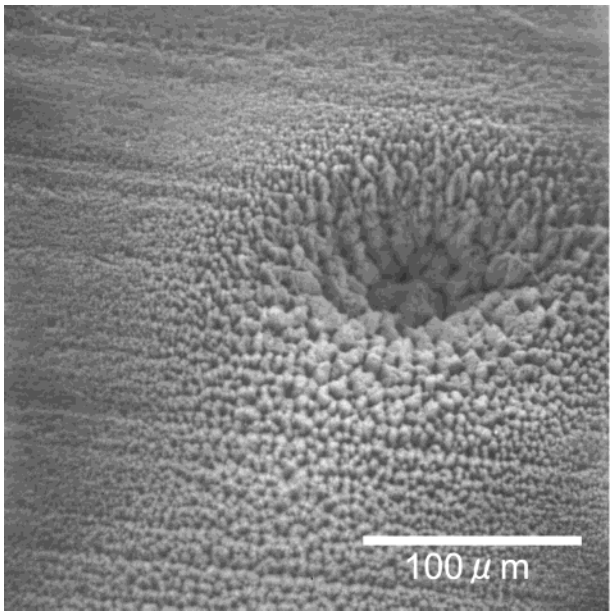

Figure 5. The SEM picture of the rutile target surface used in the PLA experiment in Figure 1. The scale bar in the picture shows 100 μm. Note that the diameter of the focused laser is about 40 μm and the small grains are piled up in the periphery.

solvated in water, they can be present as PLA species detected with UV−vis. This implies that the PLA in water involves both the forward reaction to yield solvated species and the backward reaction to yield deposited species on the target surface.

The PLA experiments were carried out in water at 275, 294, and 342 K to elucidate the solvent effect on the yield of PLA species. The absorbance values at 200 nm after PLA experiments for 30 min are plotted as a function of the ratio of temperature to viscosity of water in Figure 6. The viscosity (η) of water increases as the temperature decreases and reaches the maximum value 1.792 at 273 K. It is found that the yield of the PL species increases as the viscosity is increased. According to the Stokes−Einstein equation with respect to the mobility of not only an ion but also electronically neutral molecules in solution, the diffusion coefficient D depends on the T/η and can be expressed as follows.[71]

$$D = k_B T/6\pi\eta r_h \qquad (3)$$

Here k_B and r_h are the Boltzmann constant and hydrodynamic

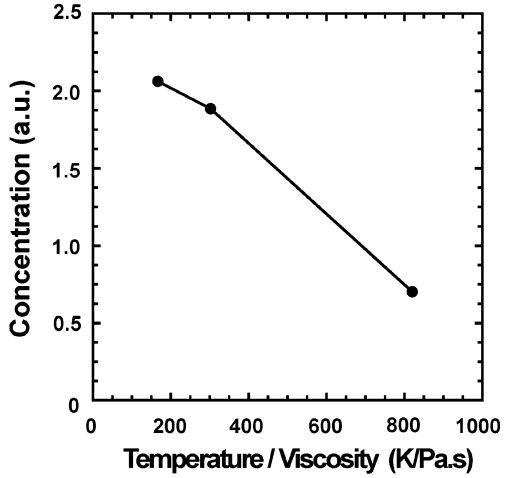

Figure 6. The concentration of the PLA species measured with UV−vis at 200 nm after 30 min of the rutile PLA experiments in water at 275, 294, and 342 K. The data are plotted as a function of the temperature divided by the viscosity of water (η), which is proportional to the diffusion coefficient. The PLA experiments were carried out in 5 mL of water with laser fluence at 65 J cm^{-2} of 10 Hz.

radius, respectively. According to the equation, the diffusion of the ions or molecules should increase when the viscosity in the solution is decreased. If the PLA species are supplied to the solution with low viscosity, they diffuse easily. However, they encounter a secondary effect such as agglomeration at high viscosity. It is noted that the yield of the PLA species in water decreases drastically with the diffusion coefficient in Figure 6 although there are only 3 data points. This result implies that the PLA species are confined in a media and suppressed not to diffuse into water solution in the initial step. If the water vapor region is formed around the rutile target in the initial PLA process, the PLA species are confined in the vapor region and no effect of water viscosity will be expected on the size of the PLA species. By the suppression in water media the size of PLA species will increase so as to be detected with UV. Considering the initial process of PLA in water, a temperature rise (ΔT) due to the pulsed laser is represented as follows[72]

$$\Delta T = (1 - R)It/C_V\rho(2D_h t)^{1/2} \qquad (4)$$

Here R, I, t, C_V, ρ, and D_h are reflectivity laser density (Wcm^{-2}), laser pulse duration time, heat capacity, density, and heat diffusivity ($\kappa = /C_V\rho$; κ is thermal conductivity), respectively. We can estimate D_h to be 3.46×10^{-2} m^2/s by using C_V (0.711 J g^{-1}K^{-1}), ρ (4.25 g cm^{-3}), and (1.05×10^{-1} J cm^{-1}s$\cdot$1 K^{-1}) for rutile TiO_2. Then ΔT reaches 7.12×10^5 K at a laser fluence 40 J cm^{-2}. We use especially $R = 0$ in this estimation since all laser light can be absorbed at 266 nm. It is noted that the temperature rise estimation can be applied to "infrared" laser experiments[72] and it does not necessarily imply that the real surface temperature can reach such extremely high temperature. If the laser spot on rutile reaches such a high temperature, the PLA flying species should encounter the surroundings as water vapor. Then no effect of water viscosity will be expected on the size of the PLA species as mentioned above. This also means that the PLA species are solvated to diffuse in water and the sizes also will be responsible for the diffusion coefficient D. When they are formed in the PLA at high water viscosity, they could be agglomerated as secondary particles so as to be detected with UV below 230 nm since the diffusion coefficient should be low. For comparison with Figures 1 and 6 it is noted that 5 mL of water was used and the laser fluence was about 65 J/cm^2

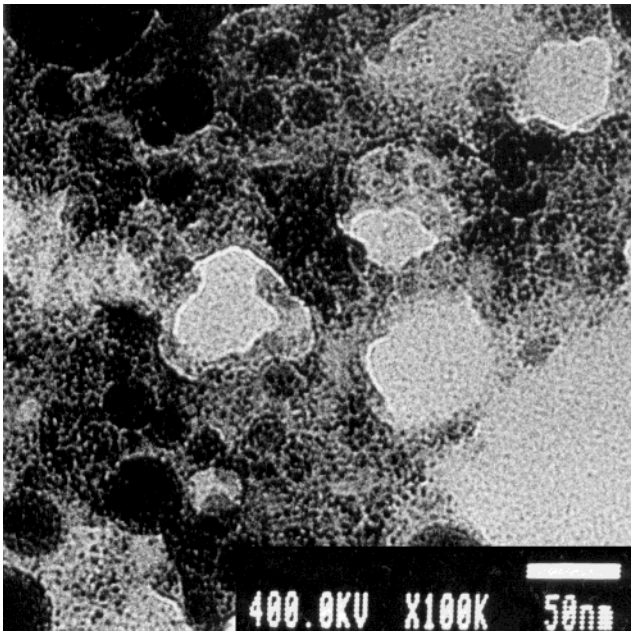

Figure 7. TEM picture of PLA species formed with laser fluence at 40 J cm^{-2} of 10 Hz for 4 h. Note that nanoparticles with a size of about 2 nm are uniformly formed and are distributed homogeneously and that they partly gather to form circle grains sized from 20 to 100 nm.

in Figure 6. The absorption edges are much larger than those detected in Figure 4. The difference arises from the laser fluence used, that is, the high band-gap PLA species are obtained at high laser fluence.

Figure 7 shows a TEM picture of the PLA species A formed in the PLA of rutile in water for 4 h with the laser fluence at 40 J cm^{-2} of 10 Hz. It is noted that nanoparticles with a size below 10 nm are uniformly formed and homogeneously dispersed and that they partly gather to form circle grains sized from 20 to 100 nm. The nanoparticles sized below 10 nm will be the PLA species A detected with UV below 230 nm and those with larger diameters will be detected at 230 to 300 nm, respectively.

When the solvated PLA species A in water were left for several days, the color of the solution changed to extremely weak light-blue. Filamentous species appeared in the water solution after an additional a few weeks. The cataphoresis was carried out to make clear the charge on the "blue" water solvated PLA species. The blue region could not be isolated on the electrode. In the used bias no water electrolysis was observed in distilled water. However, the electrolysis easily occurred in blue water. The result clearly indicates that the blue water is the electrolyte, that is, the PLA species are ionic in water. It is well-known that the titanium aquo complex $[Ti(H_2O)_6]^{3+}$ shows absorption of green due to $^2T_{2g}$ to ^2E_g transition in the octahedral ligand field at around 500 nm;[73,74] however, the color is purple because of the complementary color. The origin of the blue color was studied. Either photoluminescence or scattering in daylight is responsible for the color. The UV−vis spectra of the "blue" solution showed no other peaks except the absorption band below 230 nm. The absorption below 230 nm is not responsible for the color since the PLA species solvated solution is transparent. The Hg−Xe lamp was irradiated to the blue solution and the detector was located perpendicular to the light path. If the scattering occurs in the solution, the light intensity of the applied wavelength should be enhanced. Such an experiment was carried out in the blue solution. Only the intensities can be evaluated at the wavelengths where the Hg line spectra are

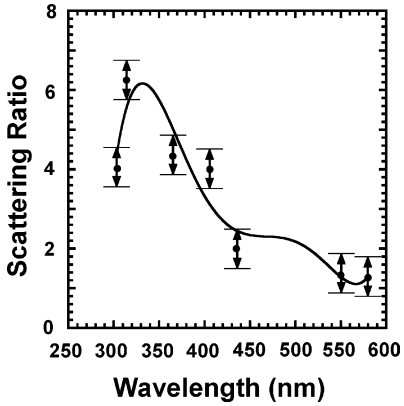

Figure 8. The scattering spectrum of the "blue" solution formed after several days of the PLA experiment in Figure 1. The scattered ratio represents how much the intensities are increased by scattered light at selected wavelengths of Hg line spectra.

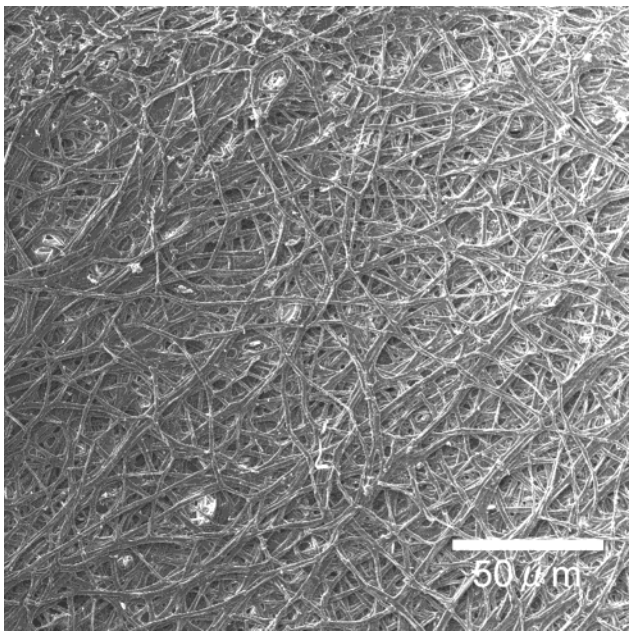

Figure 9. The SEM picture of the filamentous species detected after 4 weeks of the PLA experiment in Figure 1. The magnification is 400× and the scale bar shown right below represents 10 μm.

observed. The scattering was very weak and the spectra were integrated for 30 min. As shown in Figure 8, the light with wavelength of 300 to 440 nm is selectively scattered in the solution. This scattering in the blue region is responsible for the color. The wavelength of the scattered light is reflected by the particle size of TiO_2. The titania with a particle size below 200 nm selectively scatter the blue region light.[75] Empirical equations have been studied on the relation between the particle size D_{opt} optimized for light scattered and the wavelength λ.[76−79] It is found that the light scattering is effective when the diameter is in the same order as λ (Mie scattering). It is suggested that the D_{opt} will be obtained at about $\lambda/2$. If this holds true, D_{opt} is probably 150−200 nm in our case. As shown in Figure 7, agglomerated species with a size of about 100 nm can be measured. It is imagined that the size will be increased in water solution to reach 150−200 nm, which shows the blue light scattering.

The filamentous species were formed when the PLA species were left in the dark for several weeks. These species were deposited on a quartz substrate and dried at 358 K. Then the thin film was obtained. As shown in Figure 9 the 400×

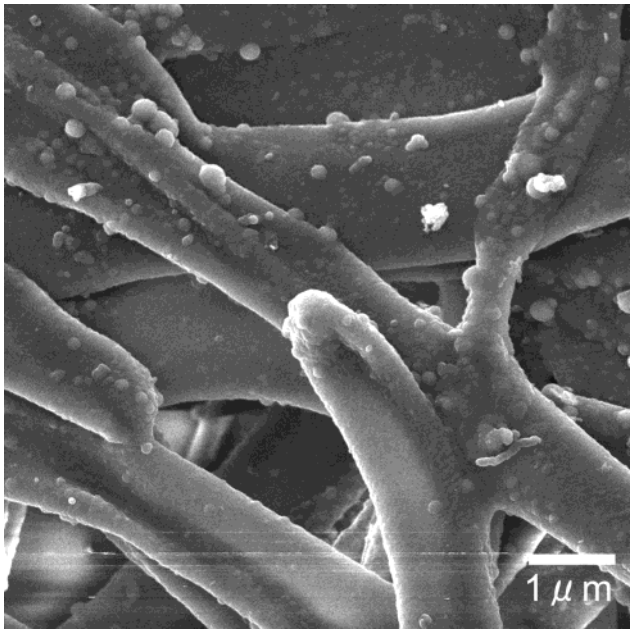

Figure 10. The magnified SEM picture of the filamentous species shown in Figure 9. The magnification is 10000× and the scale bar shown right below represents 1 μm.

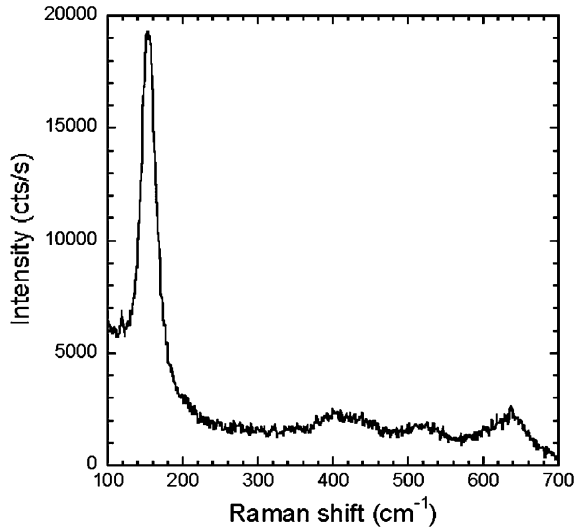

Figure 11. The Raman spectrum of the filamentous species detected after 4 weeks of the PLA experiment shown in Figure 1. The same thin film sample was used for Figures 9, 10, and 11.

magnified SEM picture reveals that these species have a network structure like net melon skin. It is noted that the diameter of the lines seems constant at about 1 μm. For more information about the fine structure of the network moiety the 10000× magnified SEM picture is shown in Figure 10. The small particles at about 100−300 nm can be seen and they are incorporated in the side of fibers to grow the diameter. They are already the secondary particles as a result of agglomeration of the PLA species A in water. At the same time they gather at the truncated terminal of the fiber to grow the fiber length. It is quite significant to note that the fiber diameter is limited to about 1 μm whereas the PLA nanoparticles grow two-dimensionally, length and width. Figure 11 shows the Raman result of the thin film. The Raman peaks are observed at around 150, 400, 520 and 640 cm^{-1}. Six Raman active fundamental modes are recorded in anatase at 144 (E_g), 397 (B_{1g}), 518 (A_{1g} and B_{1g} unresolved), and 640 cm^{-1} (E_g).[80] On the other hand, three Raman active modes should be detected in rutile at 144

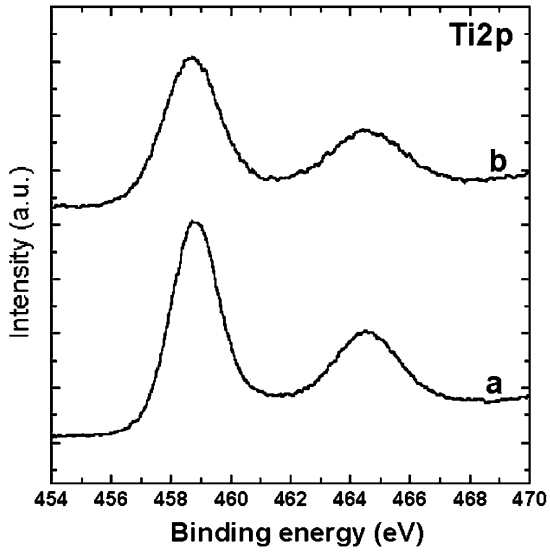

Figure 12. The Ti 2p XPS spectra of (a) rutile (010) single crystal and (b) the filamentous PLA species detected after 4 weeks of the PLA experiment in Figure 1. Note that the filamentous species are piled up enough to cover the quartz substrate and no XPS signals were detected from quartz.

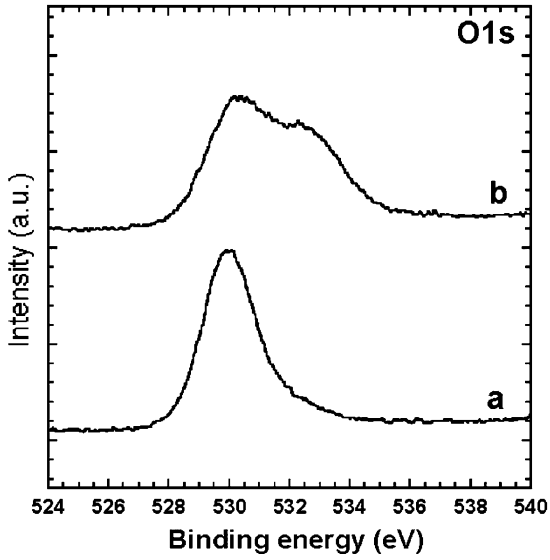

Figure 13. The O1s XPS spectra of (a) rutile (010) single crystal and (b) the filamentous species detected after 4 weeks of the PLA experiment in Figure 1. Note that the filamentous species are piled up enough to cover the quartz substrate and no XPS signals were detected from quartz.

(B_{1g}), 448 (E_g), and 613 cm^{-1} (A_{1g}). It is clear that the film is composed of both anatase and rutile forms of TiO_2 and the former is dominant. The weak broader peaks in the high-frequency region indicate a lack of short-range order.[81] The lowest frequency E_g mode of anatase form is known to be related to the grain size of the titania nanocrystals. The blue shift in frequency of the E_g mode to 150 cm^{-1} and the increase in line width are associated with a decrease of grain size.[81,82]

Figures 12 and 13 show the core XPS spectra of the Ti 2p and the O 1s bands of the thin film of filamentous PLA species. For comparison those XPS spectra of rutile TiO_2 single crystal (010) surface are shown. The thin film and the (010) surface had been exposed to air and no further treatment was carried out except evacuation at 298 K. Due to the final relaxation effect during photoelectron ejection binding energy (BE) values shifted to higher values, which is called charge-up. The BE values of

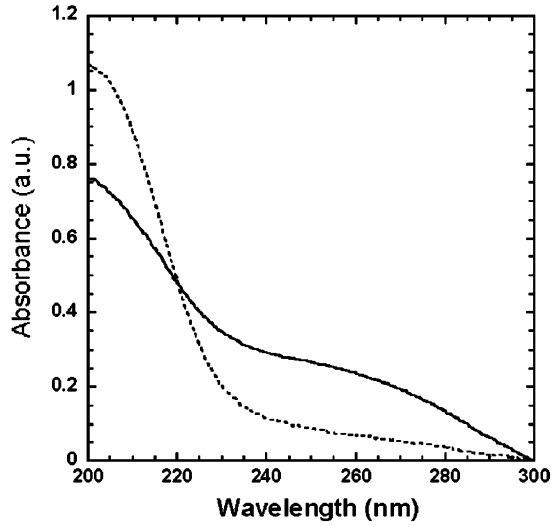

Figure 14. The absorption spectrum of the PLA solution after removing the filamentous species detected 4 weeks after the PLA experiment in Figure 1. The same absorption spectrum as that of the PLA solution 4 h later than in Figure 1 is shown for comparison.

C 1s of the samples are referenced to be 285.6 eV to estimate the amount of charge-up. Then the BE values of Ti 2p became 459.1 and 458.9 eV for the thin film and the rutile (010) surface, respectively. These values are quite similar to those of tetravalent Ti ion in TiO_2.[21,29,83] As shown in Figure 12, the BE value of Ti $2p_{3/2}$ in the film of PLA filamentous species corresponds to that of Ti^{4+} in TiO_2 and the full width at half-maximum (fwhm) value is 2.2 eV, which is close to the 2.0 eV for the (010) surface. The peak-to-peak difference between Ti $2p_{3/2}$ and Ti $2p_{1/2}$ due to the spin−orbit interaction is also the same as the (010) surface. However, O 1s spectra are quite different. The BE value of the (010) surface is 530 eV, which is the same as the reported value.[21,29,83] The O 1s spectrum of the PLA filamentous film can be deconvoluted to two components with peak BE values at 530.7 and 533.0 eV, both with 2.5 eV fwhm values. The intensity ratio is about 3:2. It is easily found that an excess amount of oxygen atom is involved in the PLA filamentous film. The atomic ratio of O to Ti is 3.2 while that of the (010) surface is 2.0. The small shoulder at 532.1 eV on the (010) surface implies that the surface is partially covered with hydroxide OH groups.[84,85] The PLA filamentous film was dried in air at 333 K, a lower temperature to remove water if present as lattice water. It is noted that the spectroscopic areas of O 1s at 530.7 eV and Ti $2p_{3/2}$ can derive the atomic ratio of O to Ti of 1.94 (almost 2.0: TiO_2), assuming the atomic sensitivity factors of 0.66 and 1.2.[84] As a result, the chemical formula of the PLA filamentous film is $TiO_2 \cdot 1.3H_2O$.

The process of how the PLA species grow up to the filamentous species is studied. The solution in Figure 1 was left for 4 weeks, and then the filamentous species appeared in the solution. The filamentous species were picked up and was mounted on the quartz substrate, which was analyzed with Raman and XPS. The UV spectrum of the water solution after removing the filamentous species is shown in Figure 14. For comparison, the UV spectrum after 4 h of the PLA experiment of rutile surfaces in Figure 1 is also shown. It is noted that the absorption intensity at around 250−300 nm increases a great deal and the absorption edge remains at a short wavelength. The absorbance increase at around 260 nm will be reflected by the formation of precursor species for the filamentous species.

In this article three different species are present: species A (PLA species in water with an absorption peaked at around 200 nm), species B (the light-blue scattering species, which will be the precursor species to agglomerated species with absorption maximum at around 260 nm), and species C (the filamentous species). Species B will be about 100 nm, which can be directly measured with SEM pictures. It is also clear the species C is the titania species, which can be proved with Raman and XPS spectroscopy. During the time course the particle size of titania species seems to grow. As the size changes the band gap also changes. As mentioned below quantum-size effects in titania nanoparticles are crucial to study. Therefore, first of all the origin of species A should be discussed. Crystalline titania nanoparticles can be easily prepared with room-temperature hydrolysis of $TiCl_4$[29,31,86] and $Ti(OC_3H_7)_4$.[26,27,87] In a weak acidic media the formation of $Ti(OH)_4$ has been suggested in the hydrolysis of $TiCl_4$.[88,89] However, it was pointed out that Ti^{4+}, $Ti(OH)^{3+}$, and $Ti(OH)_2^{2+}$ species are detectable and the last species are dominant in extremely acidic (pH <1) chloride solutions.[90] The absorption spectrum of $Ti(OH)_2^{2+}$ species ranges over 200 to 350 nm. It is well-known that $[Ti(H_2O)_6]^{3+}$ shows an absorption band at around 500 nm for the d-orbital splitting.[73,74] However, according to ligand-field theory, the d-orbital splitting between E_g and T_{2g} in octahedral symmetry is larger than that in the tetrahedral symmetry and the ligand-field effect of the water molecule is much more intense than that of OH group. Therefore, tetrahedral $Ti(OH)_4$ species should show a lower excitation energy for the d-splitting than $[Ti(H_2O)_6]^{3+}$ in addition to the small redox potential between Ti^{4+} and Ti^{3+} (0.2 eV) in acidic solution.[90] As a conclusion, the species A should not be the $Ti(OH)_4$ species. The UV/vis spectra detected at our rutile PLA experiments in water will be assigned to titania cluster species. They will be solvated in water to be stabilized and form species A with a size below 10 nm after condensation due to evaporation of water. As seen in Figure 14, such a species can be present together with the agglomerated species, which are the precursors for filamentous titania species.

In the present paper, the PLA species in water are assigned to titania cluster species. According to our results, the band-gap reaches over 5 eV. Then, the increased band-gap can be explained by the quantum confinement effect although only a small shift has been observed in titania nanoparticles[13,29,31,83,91] except for a relatively large shift as much as 0.4 to 0.6 eV for nanoparticles prepared in water-in-oil microemulsion.[92] According to the simple quantum confinement effect, band-gap energy of a cluster ($E_g^{cluster}$) can be expressed as follows[93]

$$(E_g^{cluster} = E_g^{solid} + h^2\alpha_{ln}^2/8\pi^2\mu R^2 - \beta e^2/\epsilon_r R) \qquad (5)$$

Here E_g^{solid} is the band-gap of the solid, and the second and the third term represent the quantum localization term and the correction term due to Coulomb interaction as derived from Brus.[62,91,92] The α_{ln} becomes π with $l = 0$, $n = 0$ for the 1s orbital. In addition, h, μ, R, and ϵ_r indicate Plank's constant, the effective reduced mass (equal to $m_e^* m_h^*/(m_e^* + m_h^*)$, where m_e^* and m_h^* are effective masses for the electron and the hole), the radius of the particle assumed to be spherical, and the dielectric constant of the particle, respectively. In the third term, the β is a numerical factor that takes the value 1.8 for the ns−ns transitions. The Coulomn interaction energy takes either the larger value $e^2/\epsilon_r R$ or $e^2/\epsilon_r a_B$.[93] Here a_B is Bohr radius of the Wannier exciton ($\epsilon_0\epsilon_r h^2/\pi\mu e^2$), where ϵ_0 is the vacuum permittivity. As the kinetic confinement energy of the carriers can be expected as $h^2/4\pi^2 m_e^*(m_h^*)R^2$, the Coulomn interaction energy should be smaller than the confinement energy in the case of $R \ll a_B$. This case holds true to the effective mass approximation (denoted as EMA) in semiconductor nanocrystals, that is, the

strong confinement occurs and the Coulomn interaction term can be omitted. The values of m_e* are reported to be $5m_e$ to $13m_e$[94] or $30m_e$[95] in titania nanoparticles. Here m_e is the static mass of the electron. On the other hand, those of m_h* are estimated to be about 2 m_e[86] or $>3m_e$[96] and are directly measured to be 0.8 m_e.[97] Since it has been measured that m_e* is usually larger than m_h*, μ can then be assumed to be equal to m_h*. The radii R in our PLD titania nanoparticles can be estimated from the second term in eq 5. Assuming that μ is $0.8m_e$ and E_g^{solid} is 3.2 eV for anatase, R corresponds to 0.5 and 0.4 nm for the $E_g^{cluster}$ at 5 and 6 eV, respectively. The diameter should correspond to about 1 nm for titania clusters in our experiments. It has been reported that the exciton radii α in titania nanoparticles reach 0.75−1.9 nm[86] by the relation $\alpha = \epsilon_r a_o m_e/m_e$*,[98] where a_o is the Bohr radius of the H atom. They use $\epsilon_r = 184$ for bulk TiO_2 and a m_e* of 5−13 m_e. If they use $\epsilon_r = 12$[97] for titania nanoparticles, α becomes far lower than the nanosized radius R and no quantum confinement should be expected. Assuming that μ corresponds to m_h* ($0.8m_e$) and ϵ_r takes 12, a_B becomes 0.8 nm and then the strong confinement of exciton should be expected. When the small clusters below 1 nm can be prepared, such a cluster should have a compact structure of high symmetry tending to maximize the number of chemical bonds.[62,99] As mentioned before, the PLA species A with a size below 10 nm detected with TEM pictures already will be the secondary species. They will be composed of the initially formed solvated titania clusters. Consequently the strong confinement of exciton can be expected when the radius of the primary formed PLA species is below 0.8 nm in our experiments. On the other hand, the filamentous titania species C as shown in Figure 7 yields the thin film whose band-gap is the typical value for anatase because the effective mass of electron m_e* in titania thin films is not so small ($0.71m_e$ to $1.26m_e$) that no quantum confinement effect will be expected.[48,100]

References and Notes

(1) Fujishima, A.; Honda, K. *Nature*, **1972**, *238*, 37.
(2) Fujishima, M.; Satoh, Y.; Osa, T. *Nature*, **1981**, *293*, 206.
(3) Sakata, T.; Hashimoto, K. *Nouv. J. Chem.* **1985**, *9*, 699.
(4) Miles, A.; Davies, R. H.; Worsley, D. *Chem. Soc. Rev.* **1993**, *22*, 417.
(5) O'Regan, B.; Grätzel, M. *Nature*, **1991**, *353*, 737.
(6) Nazeeruddin, M. K.; Kay, A.; Rodicio, I.; Humphry-Baker, R.; Muller, E.; Liska, P.; Vlachopoulos, N.; Grätzel, M. *J. Am. Chem. Soc.* **1993**, *115*, 6382.
(7) Vlachopoulos, N.; Liska, P.; Grätzel, M. *J. Am. Chem. Soc.* **1988**, *110*, 1216.
(8) Hagfeldt, A.; Grätzel, M. *Acc. Chem. Res.* **2000**, *33*, 269.
(9) Serpone, N.; Khairutdinov, R. F. *Stud. Surf. Sci. Catal.* **1997**, *103*, 417.
(10) Serpone, N.; Salinaro, A.; Emeline, A.; Ryabchuk, V. J. *Photochem. Photobiol. A* **2000**, *130*, 83.
(11) Alfano, O. M.; Bahnemann, D.; Cassano, A. E.; Dillert, R.; Goslich, R. *Catal. Today* **2000**, *58*, 199.
(12) Serpone, N.; Texier, I.; Emeline, A. V.; Pichat, P.; Hidaka, H.; Zhao, J. *J. Photochem. Photobiol. A* **2000**, *136*, 145.
(13) Anpo, M. *Catal. Surv. Jpn.* **1997**, *1*, 169.
(14) Asahi, R.; Morikawa, T.; Ohwaki, T.; Aoki, K.; Taga, Y. *Science* **2001**, *293*, 269.
(15) Umebayashi, T.; Yamaki, T.; Itoh, H.; Asai, K. *Appl. Phys. Lett.* **2002**, *81*, 454.
(16) Khan, S. U. M.; Al-Shahry, M.; Ingler, W. B., Jr. *Science* **2002**, *297*, 2243.
(17) Tanaka, K.; Tanaka, K.-I.; Miyahara, K. *J. Chem. Soc., Chem. Commun.* **1979**, 314.
(18) Tanaka, K.; Miyahara, K.; Tanaka, K.-I. *J. Mol. Catal.* **1982**, *15*, 133.
(19) Tanaka, K., Tanaka, K.-I. *J. Chem. Soc., Chem. Commun.* **1984**, 748.
(20) Tanaka, K.; Tanaka, K.-I.; Takeo, H.; Matsumura, C. *J. Am. Chem. Soc.* **1987**, *109*, 2422.
(21) Tanaka, K.; Miyahara, K.; Toyoshima, I. *J. Phys. Chem.* **1984**, *88*, 3504.
(22) Banfi, G.; Degiogio, V.; Ricard, D. *Adv. Phys.* **1998**, *47*, 447.
(23) Xia, Y.; Whitesides, G. M. *Angew. Chem., Int. Ed.* **1998**, *37*, 550.
(24) Burmeister, F.; Schafle, C.; Kielhofer, B.; Bechinger, C.; Boneberg, J.; Leiderer, P. *Adv. Mater.* **1998**, *10*, 495.
(25) Shklover, V.; Nazeeruddin, M.-K.; Barbe, C.; Kay, A.; Haibach, T.; Steurer, W.; Hermann, R.; Nissen, H.-U.; Grätzel, M. *Chem. Mater.* **1997**, *9*, 430.
(26) Yoldas, B. E. *J. Mater. Sci.* **1986**, *21*, 1087.
(27) Kotov, K.; Meldrum, F.; Fendler, J. H. *J. Phys. Chem.* **1994**, *98*, 8827.
(28) Skinner, D. E.; Colombo, D. P., Jr.; Cavaleri, J. J.; Bowman, R. M. *J. Phys. Chem.* **1995**, *99*, 7853.
(29) Kumar, P. M.; Badrinarayanan, S.; Sastry, M. *Thin Solid Films* **2000**, *358*, 122.
(30) Tanaka, K.; Miyahara, K.; Tanaka, K.-I. *Bull. Chem. Soc. Jpn.* **1981**, *54*, 3106.
(31) Serpone, N.; Lawless, D.; Khairutdinov, R. *J. Phys. Chem.* **1995**, *99*, 16646.
(32) Arnal, P.; Corriu, R. J. P.; Leclercq, D.; Mutin, P. M.; Vioux, A. *Chem. Mater.* **1997**, *9*, 694.
(33) Li, D.; Xia, Y. *Nano Lett.* **2003**, *3*, 555.
(34) Arabatzis, I. M.; Falaras, P. *Nano Lett.* **2003**, *3*, 249.
(35) Yi, D. K.; Kim, D.-Y. *Nano Lett.* **2003**, *3*, 207.
(36) Cheung, J. T.; Sankur, H. *CRC Cri. Rev. Solid State Sci.* **1988**, *15*, 63.
(37) *Laser Ablation*: *Mechanism and Applications-II*; Miller, J. C., Geohegan, D. B., Eds.; AIP Conf. Proc. No. 288; AIP: New York, 1994.
(38) Loundes, D. H.; Geohegan, D. B.; Puretzky, A. A.; Norton, D. P.; Rouleau, C. M. *Science* **1996**, *273*, 898.
(39) Morales, A. M.; Lieber, C. M. *Science* **1998**, *279*, 208.
(40) Blanchet, G. B.; Fincher, C. R., Jr.; Jackson, C. L.; Shah, S. I.; Gardner, K. H. *Science* **1993**, *262*, 719.
(41) Tanaka, K.; Yokota, N.; Shirai, N.; Zhuang, Q.; Nakata, R. *Appl. Surf. Sci.* **1996**, *100/101*, 264.
(42) Tanaka, K.; Shirai, N.; Sugiyama, I.; Nakata, R. *Nucl. Instrum. Methods Phys. Res. B* **1997**, *121*, 401.
(43) Tanaka, K. *Appl. Surf. Sci.* **1998**, *279*, 208.
(44) Tanaka, K.; Sonobe, D. *Appl. Surf. Sci.* **1999**, *140*, 138.
(45) Tanaka, K.; Ohga, K.; Choo, C.-K.; Nakata, R. *J. Appl. Phys.* **2001**, *90*, 5369.
(46) Tanaka, K.; Fukui, K.; Ohga, K.; Choo, C.-K. *J. Vac. Sci. Technol. A* **2002**, *20*, 486.
(47) Nakamura, I.; Negishi, N.; Kutsuna, S.; Ihara, T.; Sugihara, S.; Takeuchi, K. *J. Mol. Catal. A* **2000**, *161*, 205.
(48) Choi, Y.; Yamamoto, S.; Saitoh, H.; Sumita, T.; Itoh, H. *Nucl. Instrum. Methods Phys. Res., Sect. B* **2003**, *206*, 241.
(49) Tang, H.; Prasad, K.; Sanjines, R.; Schmid, P. E.; Levy, F. *J. Appl. Phys.* **1994**, *75*, 2042.
(50) Okubo, N.; Nakazawa, T.; Katano, Y.; Yoshizawa, I. *Appl. Surf. Sci.* **2002**, *197*−*198*, 679.
(51) Koshizaki, N.; Narazaki, A.; Sasaki, T. *Appl. Surf. Sci.* **2002**, *197*−*198*, 624.
(52) Hirasawa, M.; Seto, T.; Orii, T.; Aya, N.; Shimura, H. *Appl. Surf. Sci.* **2002**, *197*−*198*, 661.
(53) Moret, M. P.; Zallen, R.; Vijay, D. P.; Desu, S. B. *Thin Solid Films* **2000**, *366*, 8.
(54) Sasaki, T.; Koshizaki, N.; Beck, K. M. *Appl. Phys. A* **1999**, *69*, S771.
(55) Yoon, J.-W.; Sasaki, T.; Koshizaki, N.; Traversa, E. *Scr. Mater.* **2001**, *44*, 1865.
(56) Sasaki, T.; Koshizaki, N.; Terauchi, S.; Umehara, H.; Matsumoto, Y.; Koinuma, M. *Nanostruct. Mater.* **1997**, *8*, 1077.
(57) Beck, K. M.; Sasaki, T.; Koshizaki, N. *Chem. Phys. Lett.* **1999**, *301*, 336.
(58) Sasaki, T.; Beck, K. M.; Koshizaki, N. *Appl. Surf. Sci.* **2002**, *197*−*198*, 619.
(59) Brugger, P. A.; Cuender, P.; Grätzel, M. *J. Am. Chem. Soc.* **1981**, *103*, 2923.
(60) Rossetti, R.; Hull, R.; Gibson, J. M.; Brus, L. E. *J. Chem. Phys.* **1985**, *82*, 552.
(61) Mews, A.; Eychmüller, A.; Giersig, M.; Schooss, D.; Weller, H. *J. Phys. Chem.* **1994**, *98*, 934.
(62) Brus, L. E. *J. Phys. Chem.* **1994**, *98*, 3575.
(63) Hines, M. A.; Guyot-Sionnest, P. *J. Phys. Chem.* **1996**, *100*, 468.
(64) Kamalov, V. F.; Little, R.; Logunov, S. L.; El-Sayed, M. A. *J. Phys. Chem.* **1996**, *100*, 6381.
(65) Ahmadi, T. S.; Wang, Z. L.; Green, T. C.; Henglein, A.; El-Sayed, M. A. *Science* **1996**, *272*, 1924.
(66) Yeh, M.-S.; Yang, Y.-S.; Lee, Y.-P.; Lee, H.-F.; Yeh, Y.-H.; Yeh, C.-S. *J. Phys. Chem. B* **1999**, *103*, 6851.

(67) Sibbard, M. S.; Chumanov, G.; Cotton, T. M. *J. Phys. Chem.* **1996**, *100*, 4672.
(68) Mafune, F.; Kohno, J.; Takeda, Y.; Kondow, T.; Sawabe, H. *J. Phys. Chem.* **2000**, *104*, 8333.
(69) Mafune, F.; Kohno, J.; Takeda, Y.; Kondow, T.; Sawabe, H. *J. Phys. Chem.* **2000**, *104*, 9111.
(70) Pankove, J. I. *Optical Processes in Semiconductors*; Dover: New York, 1971; Chapter 3.
(71) Atkins, P. W. *Physical Chemistry*, 6th ed.; Oxford University Press: Oxford, UK, 1998; p 749.
(72) Cheung, J. T.; Sankur, H. *CRC Crit. Rev. Solid State Mater. Sci.* **1988**, *15*, 63.
(73) Orgel, L. E. *An Introduction to Transition Metal Chemistry*: *Ligand Field Theory*, 2nd ed.; Wiley: New York, 1966; p 35.
(74) Ballhausen, C. J. *Introduction to Ligand Field Theory*; McGraw-Hill: New York, 1962; p 227.
(75) Bruehlman, R. J.; Thomas, L. W.; Gonick, E. *Off. Dig.* **1961**, *33*, 252.
(76) Jaenicke, W. *Z. Elektrochemie* **1956**, *60*, 163.
(77) Weber, H. H.; Gerhards, J. *Farbe + Lack* **1961**, *67*, 434.
(78) Mitton, P. B. *Off. Dig.* **1962**, *34*, 73.
(79) Steig, F. B. *J. Oil Colour Chem. Assoc.* **1970**, *53*, 469.
(80) Roberts, T. D.; Laude, L. D.; Geskin, V. M.; Lazzaroni, R.; Gouttebaron, R. *Thin Sold Films* **2003**, *440*, 268.
(81) Zhang, W. F.; Zhang, M. S.; Yin, Z.; Chen, Q. *Appl. Phys. B* **2000**, *70*, 261.
(82) Bessani, D.; Lottici, P. P.; Ding, X. Z. *Appl. Phys. Lett.* **1998**, *72*, 73.
(83) Bribbs, D.; Seah, M. P. *Practical Surface Analysis*, 1st ed.; John Wiley: New York, 1984; p 493.
(84) Carley, A. F.; Spoto, G.; Chalker, P. R.; Riviere, J. C.; Roberts, M. W. *J. Chem. Soc., Faraday Trans. 1* **1987**, *83*, 351.
(85) Pouilleau, J.; Devilliers, D.; Groult, H.; Marcus, P. *J. Mater. Sci.* **1998**, *32*, 5645.
(86) Kormann, C.; Bahnemann, D. W.; Hoffmann, M. R. *J. Phys. Chem.* **1988**, *92*, 5196.
(87) Choi, W.; Termin, A.; Hoffmann, M. R. *J. Phys. Chem.* **1994**, *98*, 13669.
(88) Babko, A. K.; Gridchina, G. I.; Nabivanets, B. I. *Russ. J. Inorg. Chem.* **1962**, *7*, 66.
(89) Nabivanets, B. I.; Lukachina, V. V. *Ukr. Khim. Zh.* **1964**, *30*, 1123.
(90) Ciavatta, L.; Ferri, D.; Riccio, G. *Polyhedron* **1985**, *4*, 15.
(91) Brus, L. E. *J. Chem. Phys.* **1984**, *80*, 4403.
(92) Joselevich, E.; Willner, I. *J. Phys. Chem.* **1994**, *98*, 7628.
(93) Banfi, J.; Degigiorgio, V. *Adv. Phys.* **1998**, *47*, 447.
(94) Pascual, J.; Camassel, J.; Mathieu, H. *Phys. Rev. B* **1978**, *18*, 5606.
(95) Bordreaux, D. S.; Williams, F.; Nozik, A. J. *J. Appl. Phys.* **1980**, *51*, 2158.
(96) Kasinski, J. J.; Gomez-Jahn, L. A.; Faran, K. J.; Gracewski, S. M.; Dwayne Miller, R. J. *J. Chem. Phys.* **1989**, *90*, 1253.
(97) Enright, B.; Fitzmaurice, D. *J. Phys. Chem.* **1996**, *100*, 1027.
(98) Brus, L. E. *J. Phys. Chem.* **1986**, *90*, 2555.
(99) Jarrold, M. A. *Science* **1991**, *252*, 1085.
(100) Stamate, M. D. *Appl. Surf. Sci.* **2003**, *205*, 353.